Fusion Engineering and Design 192 (2023) 113620

Contents lists available at ScienceDirect

Fusion Engineering and Design

journal homepage: www.elsevier.com/locate/fusengdes

Retention of noble and rare isotope gases in plasma-facing components – Experience from the JET tokamak with the ITER-like wall

Laura Dittrich [a,*], Per Petersson [a], Sunwoo Moon [a], Marek Rubel [a], Tuan Thien Tran [b], Anna Widdowson [c], JET Contributors[1]

[a] Fusion Plasma Physics, KTH Royal Institute of Technology, 100 44 Stockholm, Sweden
[b] Department of Physics and Astronomy, Uppsala University, 751 20 Uppsala, Sweden
[c] Culham Centre for Fusion Energy, Abingdon, Oxfordshire OX14 3DB, United Kingdom

ARTICLE INFO

Keywords:
Plasma-wall interactions
Seeded gases
Plasma-facing materials
JET tokamak
ITER-like wall

ABSTRACT

Plasma edge cooling, ion cyclotron wall conditioning and disruption mitigation techniques involve massive gas injection (by puffs or pellets) to the torus. A certain fraction remains in plasma-facing components (PFC) due to co-deposition and implantation. An uncontrolled release/desorption of such retained species affects the stability of plasma operation. The aim of this work was to determine the lateral and depth distribution of noble (^{3}He, ^{4}He, Ne, Ar), seeded (N_2, Ne, Ar) and tracer gases (^{15}N, ^{18}O) in PFC retrieved from the JET tokamak with the ITER-Like Wall (JET-ILW) after three experimental campaigns (ILW-1, ILW-2, ILW-3). Results regarding the retention of those gases are shown as well as a comparison to the deuterium retention in the studied areas. Heavy ion elastic recoil detection analysis was used, being the only technique capable of detection and quantitative assessment of all elements, especially low-Z isotopes. Helium was found on the divertor Tile 5, locally up to $44{\cdot}10^{15}$ ^{3}He cm^{-2} and $12{\cdot}10^{15}$ ^{4}He cm^{-2}, and on the limiters as well. Neon was found in two positions on the limiters, with up to $10{\cdot}10^{15}$ Ne cm^{-2} and the ^{15}N tracer on Be limiters exposed to ILW-3. A correlation of N retention with the N seeding rates for each campaign has also been found.

1. Introduction

A variety of gases are injected into the JET tokamak plasma during operation. Besides hydrogen isotopes used as fuel (especially deuterium) other species have a wide range of applications: e.g. plasma edge cooling, disruption mitigation, ion cyclotron resonance heating scenarios and wall conditioning. Rare isotopes are also injected for research purposes to verify hypotheses on material migration and in-vessel interaction with wall components. Most of the injected gases are pumped out by the gas handling systems, however a fraction is temporarily or long-term trapped in the torus and deposited on plasma-facing components (PFC). If medium-Z or high-Z gases were released uncontrolled during a discharge, it could impact plasma stability and lead to a disruption in a tokamak [1]. In a future reactor-class D-T machine the use of certain high-Z gases can also lead to activation as some long-lived radioactive transmutation products could be created, e.g. ^{85}Kr (krypton) decaying to ^{85}Rb (rubidium) with a half-life of 17.78 years. Therefore, the retention and spatial distribution needs to be thoroughly studied to enable predictions for a safe and economically viable reactor operation.

The Joint European Torus with the ITER-like wall (JET-ILW) is a large-scale test bed to develop operational scenarios for ITER [2]. The full metal JET-ILW comprises arrays of beryllium (Be) limiters and Be coatings on the inner wall cladding in the main chamber, and tungsten (W) in the divertor, as bulk metal tiles and W coatings on carbon fibre composites (W/CFC). JET-ILW operation started in 2011. Three major campaigns were performed after which PFC and wall probes were retrieved during scheduled shutdowns: 2011–2012 (ILW-1), 2013–2014 (ILW-2) and 2015–2016 (ILW-3). Basic information about the operation is included in Table 1, while references [3,4] contain details regarding plasma interaction times with respective limiter tiles, and strike point positions in the divertor during the three ILW campaigns.

Besides the main gases, deuterium (D or ^{2}H) and protium (^{1}H), used in ILW-1 to ILW-3 as fuel, for disruption mitigation by massive gas injection (ILW-2, ILW-3) and, pellet injection [3], also other gases were used. Over the years multiple studies have been done on PFC from the JET-ILW towards the retention of hydrogen isotopes showing the

* Corresponding author.
E-mail address: lauradi@kth.se (L. Dittrich).
[1] See list of authors: J. Mailloux et al., Nucl. Fusion 62 (2022) 042026.

https://doi.org/10.1016/j.fusengdes.2023.113620
Received 31 October 2022; Received in revised form 2 February 2023; Accepted 1 March 2023
Available online 10 March 2023

Table 1
Plasma operation times and total input energy for ILW campaigns 1 to 3, data from [3,4].

Campaign	Total input energy (GJ)	Plasma time (h)		
		Limiter	Divertor	Total operation
ILW-1	150	6.0	13.0	19.0
ILW-2	201	5.2	14.2	19.4
ILW-3	245	4.9	18.5	23.4

long-term retention of about 0.2% of the total injected D fuel for JET-ILW [5,6]. Nitrogen (N_2), neon (Ne), and argon (Ar) were used for plasma edge cooling and disruption mitigation. Xenon (Xe) and Kr were tested as edge cooling agents for ITER [7,8]. Ion cyclotron resonance heating requires helium-3 (^{3}He) for minority heating scenarios, while helium-4 (^{4}He) puffing was applied in L-H transition and confinement studies, mainly in ILW-3 [9]. Carbon-containing gases (deuterated methane and acetylene) were used for calibrating divertor and main chamber diagnostics, e.g. charge exchange recombination spectroscopy (CXRS). Small amounts of rare isotopes were puffed in as markers for material migration and gas retention studies, e.g. ^{15}N (natural abundance 0.337%) in ILW-1 [10] and ILW-3, and oxygen-18 (^{18}O, natural abundance 0.205%) in ILW-3 [11]. The use of ^{15}N was motivated by the interest whether nitrogen, detected ex-situ on all studied samples of metal PFC from JET [12], was deposited in the tokamak or afterwards, i.e. during the tiles' exposure to air. Also ^{18}O was used for a similar reason, especially to address in-vessel Be oxidation. However, the knowledge on the retention of those injected noble and rare isotope species has been rather scarce, because of limited analytical capabilities (very limited number of sensitive, selective and quantitative methods) and, also by the cost of such studies.

The trapping of the injected gases, which can occur by implantation [13] in the first tens of nm of the sample surface, co-deposition [14], chemical reactions [15] and, adsorption [16] (the latter two concerning species that can have free radicals, such as H, C, N and O), was to be studied. The aim of this work was to detect and determine the distribution of light noble (He isotopes, Ne, Ar) and rare (^{15}N, ^{18}O) seeded gases in the surface region of samples retrieved from the torus after three ILW campaigns.

2. Experimental

2.1. Gases

The study was carried out for specimens retrieved from the JET-ILW vessel after the three ILW campaigns. The specimens' poloidal locations in the torus are shown in Fig. 1(a). They originate from the bulk tungsten divertor Tile 5 and arrays of bulk beryllium limiters: inner wall guard (IWGL) and outer poloidal limiters (OPL), and the upper dump plates (DP). IWGL and OPL specimens were taken from the tiles located at the midplane, where the plasma impact on those PFC is the most distinct [3,6].

The amounts of the injected gases during regular plasma operation are summarized for each species and ILW campaign in Table 2. Information about the gas inlet modules (GIM) is also included. The map of respective inlets is in Fig. 1(b). Gases injected through the disruption mitigation valves (DMV), two at the top and in the midplane plane [17,18], are shown separately in Table 2.

2.2. Tiles and specimens

The castellated Be limiters have different shapes dependent on the location in JET. The OPL Tiles 14 (specifically tile 4D14) and 15 (4D15) from Octant 4 were retrieved and analysed. These tiles have each 9 castellated rows in poloidal and 26 columns in toroidal direction, see Fig. 2(a). The OPL are divided into a centre piece and six segments: three

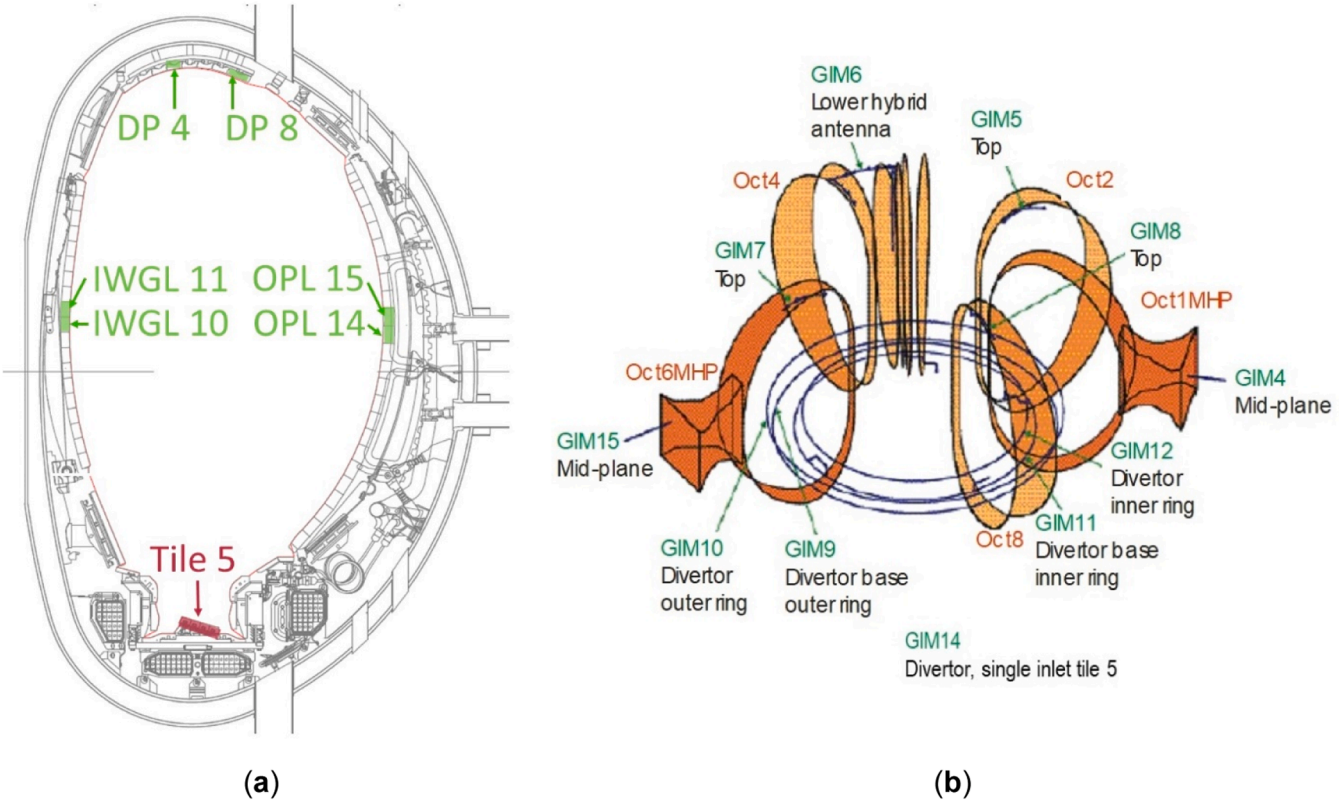

Fig. 1. (a) Cross-section of the JET tokamak with poloidal positions of retrieved tiles for analysis in colour: green for beryllium tiles, red for bulk tungsten tiles. (b) Map of GIM in the torus.

Table 2
Hydrogen isotopes, noble and other seeded gases injected during plasma discharges for ILW campaigns 1 to 3 through the GIM and DMV in number of atoms. For hydrogen isotopes the amounts for pellet injection and for deuterium additionally the neutral beam amounts are included [3]. ^{16}O and ^{14}N are present in natural abundance with concentrations of 99.757% and 99.636%, respectively. The amounts of CD_4 and C_2D_4 are given in number of molecules.

Gas	Injection point	ILW-1	ILW-2	ILW-3
^{1}H	GIM, pellets	$2.5{\cdot}10^{24}$	$2.7{\cdot}10^{25}$	$8.0{\cdot}10^{25}$
	DMV	–	$1.3{\cdot}10^{24}$	$1.0{\cdot}10^{25}$
^{2}D	GIM, pellets	$9.1{\cdot}10^{26}$	$5.8{\cdot}10^{26}$	$6.4{\cdot}10^{26}$
	DMV	–	$2.4{\cdot}10^{26}$	$1.4{\cdot}10^{26}$
^{3}He	main chamber GIM	–	$8.2{\cdot}10^{22}$	$7.4{\cdot}10^{22}$
^{4}He	main chamber GIM	–	$2.5{\cdot}10^{21}$	$3.3{\cdot}10^{22}$
CD_4	GIM 11	–	–	$3.7{\cdot}10^{23}$ [a]
C_2D_4	GIM	–	–	$4.3{\cdot}10^{21}$ [b]
^{14}N	GIM 4, 8, 11	$9.7{\cdot}10^{23}$	$3.8{\cdot}10^{24}$	$2.1{\cdot}10^{24}$
^{15}N	GIM 14, 10	$1.3{\cdot}10^{22}$ (GIM 14)	–	$8.5{\cdot}10^{23}$ (GIM 10) [c]
^{16}O	GIM 11	–	–	$2.0{\cdot}10^{22}$ [d]
^{18}O	GIM 11	–	–	$2.8{\cdot}10^{22}$
Ne	divertor GIM	$2.1{\cdot}10^{21}$	$1.2{\cdot}10^{23}$	$1.3{\cdot}10^{23}$
	DMV	–	$3.8{\cdot}10^{23}$	$1.2{\cdot}10^{24}$
Ar	divertor GIM	$2.9{\cdot}10^{21}$	$8.5{\cdot}10^{21}$	$1.3{\cdot}10^{22}$
	DMV	–	$2.0{\cdot}10^{25}$	$9.2{\cdot}10^{24}$
Kr	divertor GIM	–	–	$7.1{\cdot}10^{21}$
	DMV	–	$2.0{\cdot}10^{24}$	$1.3{\cdot}10^{25}$
Xe	divertor GIM	–	–	$7.9{\cdot}10^{19}$

[a] CD_4 was puffed in two series: $1.1{\cdot}10^{23}$ in the middle of ILW-3 and $2.6{\cdot}10^{23}$ at the last session, 8 shots before the last one.
[b] C_2D_4 puffed approx. 400 shots before the end of ILW-3.
[c] Injection during two last sessions in ILW-3.
[d] Injection during 4 shots in the penultimate ILW-3 session; 30 shots before the last discharge.

on the left and three on the right. The naming convention of the segments (from right to left in top view) is right hand (RH) wing, RH Intermediate (Int.) 1, RH Int. 2, centre, left hand (LH) Int. 2, LH Int. 1, and LH wing. In each of the segments the columns are counted right to left from column (C) 1 onward, i.e., the wings consist of C1 to C3, the Int. 1 segments of C1 to C2, the Int. 2 segments of C1 to C3 and the centre segment of C1 to C10. The rows (R) R1 to R9 are counted from the top of the tile towards the divertor. The ion drift on the OPL is moving from the LH wing in direction to the right side. The OPL Tile 14 was retrieved after exposure to ILW-1 and ILW-3, Tile 15 after ILW1–3, i.e. all three campaigns. The OPL Tiles 14 and 15 are located on the low-field side of JET. Due to the shaping of the tiles the wing segments extend furthest into the scrape-off layer (SOL), while the centre segment is the most exposed to plasma. Details on the plasma-tile interaction times for OPL and IGWL in respective campaigns are in [3].

The IWGL consist of a centre piece and two segments on the left and two on the right. The outermost segments are called wings, as for the OPL. The IWGL tiles have 8 castellated rows and 25 columns, each. The IWGL segments are called RH wing (C1 to C4), RH Int. (C1 to C3), centre (C1 to C11), LH Int. (C1 to C3), and LH wing (C1 to C4). The columns are counted for each segment from right to left in top view. IWGL Tile 10 (2XR10) was retrieved from JET after exposure to ILW-1 and ILW-2, and Tile 11 (2XR11) after ILW1–3 exposure; both from Octant 2. The IWGL tiles are located on the high-field side of the machine, approximately on the same height as the OPL. Accordingly, the ion drift is passing from the RH wing of the IWGL to the left. The tiles are shaped as well, column 6 of the centre segment is the one closest to the plasma.

The DP are arranged in so-called beams of eight tiles. The tiles become narrower towards the low-field side of the machine [19]. The rows on each tile are counted poloidally from the low-field side to the high-field side. The columns on the tile are counted toroidally in the ion drift direction. Samples from two DP, retrieved after ILW-3, were available for analysis: Tile 2B4C (ILW-3), the fourth DP from the strong-field side in beam B(C) of Octant 2, and Tile 3A8 (ILW1–3), the eighth DP in beam A in Octant 3. Tile 3A8 has 7 castellated columns and 14 rows, while Tile 2B4C is wider with 11 columns are 9 rows. The DP in JET are shaped as well, see Fig. 2(b). The centre column extends furthest into the plasma, for 2B4C the sixth column is the centre one and for 3A8 the fourth. The retrieved DP are partially molten, as can be seen in Fig. 2 (b), details about the damage are reported in [19].

The bulk tungsten Tile 5 of the divertor consists of separate modules, each with four stacks (referred to as A, B, C and D) of 24 lamellae, see Fig. 2(c). There are gaps between the single lamellae. The poloidally orientated gaps are 0.4 mm wide, while the toroidal gaps between the stacks are 1.5 mm wide. The modules are arranged in a way, that the last lamellae of the previous module are shading the couple of first lamellae of the following module. The difference in the thermal load to respective regions of the tile can be seen by the optical emission spectroscopy of the JET divertor, an example is presented in Fig. 2(b) of [20].

The retrieved tiles were cut at the Institute of Atomic Physics, in Bucharest, Romania under temperature control. The temperature was maintained below 60 °C at all times to avoid the release of fuel species.

2.3. Analysis methods

To determine the retention of the noble and seeded gases, ex-situ analyses were performed. In total 60 cut samples, including one unexposed Be reference sample, were analysed in the Tandem Laboratory in Uppsala University [21] by ion beam analysis methods. The main method was time-of-flight heavy ion elastic recoil detection analysis (ToF HIERDA) using either a bromine ($^{80}Br^{7+}$ 32 MeV) or iodine ($^{127}I^{n+}$ $n = 8$ or 10, 36 or 44 MeV) beam. The beam impinges on the sample at the angle of 22.5°, whereas the recoils are detected at 135° with respect to the incoming beam. As a consequence of the beam-target geometry, the beam spot is elliptical, approximately 1 × 3 mm. Details of the technique, signal formation, data recording and data analysis have been presented elsewhere [22]. The detection system is based on a segmented gas ionization chamber and time-of-flight detector [23]. ToF HIERDA allows the determination of atomic composition and depth profiling of respective species of up to 0.8 μm in low-Z targets (200–300 nm in W) with a depth resolution of about 20 nm. The method ensures simultaneous measurements of elements ranging from hydrogen to uranium. The obtained spectra are analysed using the POTKU software [24]. HIERDA is the only technique to probe all species in the surface layer with equal detection efficiency; the detection limit is $5{\cdot}10^{14}$ cm^{-2}. Very good mass resolution in the H to Ne range makes HIERDA particularly suited for the reported studies, e.g. it is the only means to assess simultaneously lateral and depth distributions of H, D, ^{3}He, ^{4}He, and two isotopes of N and O. There are also limitations related to surface roughness of the examined objects; this adds to the uncertainty in the results of measurements. For the depth scale and the total atomic contents integrated over areal densities all error sources sum up to an error of up to 30%, as it is explained in detail in [25]. For heavy elements the mass resolution decreases. Scattered-off ions of the primary beam (Br or I) make the analysis of, respectively, Kr and Xe challenging. Surface morphology of Be samples was determined on six selected specimens by scanning electron microscopy (SEM) by using LEO 1550 (Zeiss) equipment. The roughness of four Be samples was investigated with a Veeco Dektak 150 profiler with a 150 μm tip.

3. Results

3.1. Beryllium limiters

The study of plasma-treated limiters was preceded by the analysis of a reference Be sample cut from the unexposed limiter block. Data in Table 3 indicate the presence of oxygen (probably thin BeO surface layer and adsorbed water vapour), small amounts of adsorbed species (H, C)

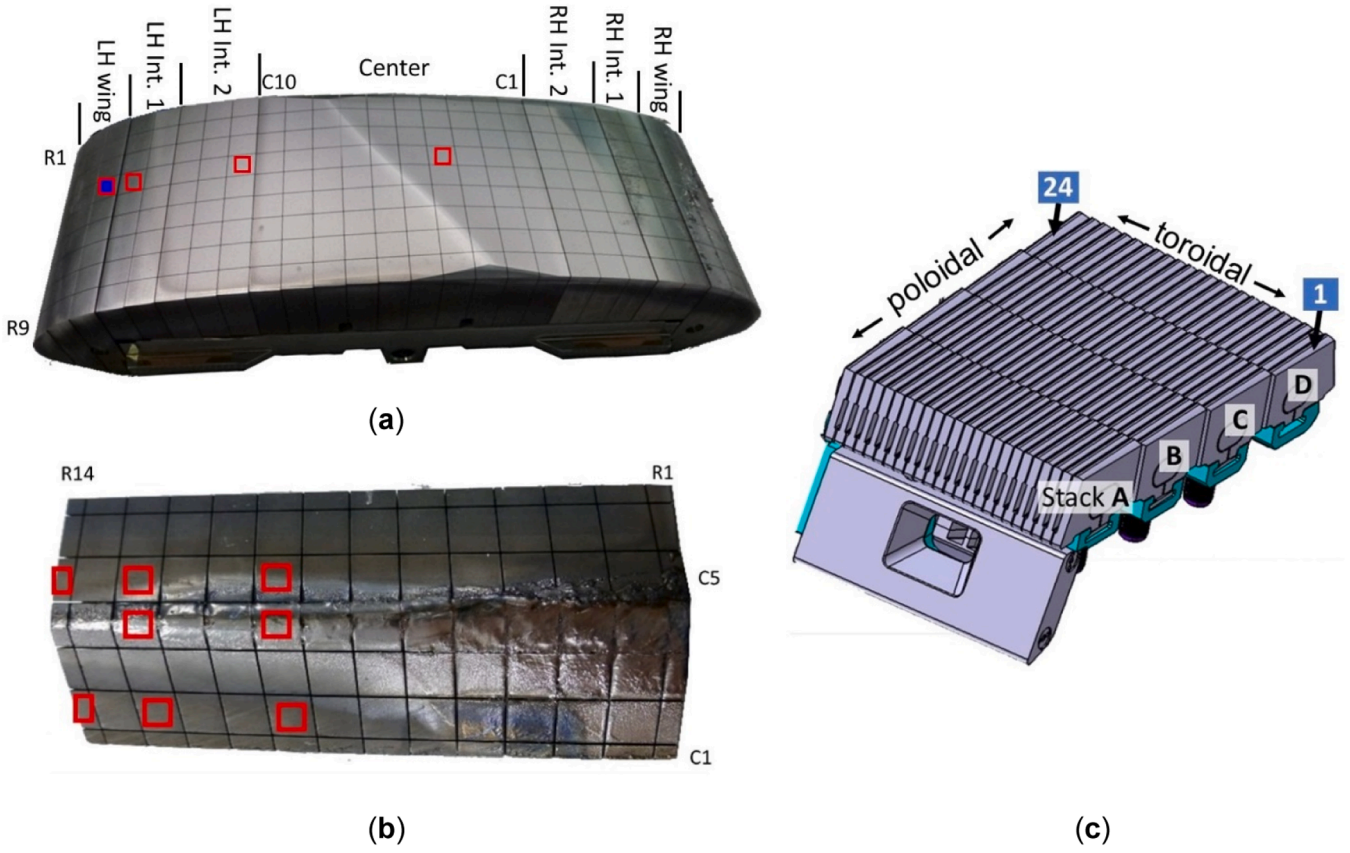

Fig. 2. (**a**) The OPL Tile 14 (4D14) with a description of the tile segments and marked positions of retrieved samples for analysis, the ILW-1 sample in blue and ILW-3 samples as red squares. (**b**) The eighth Dump Plate (3A8) with partially molten surface; row and column numbering and investigated sample positions marked in red. (**c**) Schematic drawing of the four stacks of the divertor Tile 5.

Table 3
Results of ToF HIERDA measurements on the unexposed Be reference sample. Values given in 10^{15} atoms cm^{-2}. Measurement depth is $9{\cdot}10^{18}$ atoms cm^{-2}, this corresponds to approximately 750 nm at the Be density of 1.803 g cm^{-3}.

	Areal density in 10^{15} atoms cm^{-2}							
	^{1}H	^{2}D	Be	C	N	O	Ar	Cr, Fe, Ni
Reference sample	41	–	8252	42	–	658	11	83

and steel components remaining probably after the sample machining. It is stressed that no N has been found on the surface, while Ar content reaches $11{\cdot}10^{15}$ atoms cm^{-2}. Its origin may be linked to the machining of limiter tiles in argon atmosphere. In the following, results of ex-situ analyses from six limiter positions are presented by the tile type: OPL, IWGL and DP.

3.1.1. *Outer poloidal limiters*

Table 4 contains results of ToF HIERDA measurements on plasma-facing surfaces (PFS) of the OPL samples up to a depth of $9{\cdot}10^{18}$ atoms cm^{-2}, i.e. around 750 nm assuming the Be density of 1.803 g

Table 4
ToF HIERDA measurement results on samples of OPL Tile 14 (4D14) and Tile 15 (4D15) from Octant 4 exposed to ILW-1/ILW-3 and ILW1–3, respectively. Values given in 10^{15} atoms cm^{-2}. Measurement depth $9{\cdot}10^{18}$ atoms cm^{-2}, this corresponds to approximately 750 nm at assumed density of 1.803 g cm^{-3}.

Tile	Position	Areal density in 10^{15} atoms cm^{-2}													
		^{1}H	^{2}D	^{3}He	^{4}He	Be	C	^{14}N	^{15}N	^{16}O	^{18}O	Ne	Ar	Cr, Fe, Ni, Mo	W
4D14 (ILW-1)	**LH wing C1R4**	57	170	–	–	8054	183	132	–	320	–	–	–	91	12
4D14 (ILW-3)	**LH wing C1R4**	18	74	35	–	7854	207	224	44	527	–	10	3	84	9
	LH Int. 1 C2R4	–	87	–	–	8637	68	35	19	216	–	1	–	22	1
	LH Int. 2 C1R4	9	65	–	–	8908	12	3	13	80	–	–	–	9	–
	Centre C4R4	10	32	–	–	8918	8	5	11	93	–	–	<1	20	1
4D15 (ILW1–3)	**LH wing C3R4**	49	116	–	–	7472	257	165	68	773	0	–	25	119	31
	LH wing C1R4	16	59	31	5	7818	206	226	37	567	1	3	7	101	12
	LH Int. 1 C2R4	14	79	–	–	8240	168	135	31	356	–	–	–	68	9
	LH Int. 2 C1R4	–	29	–	–	8974	8	–	13	58	–	–	–	13	–
	RH Int. 2 C3R6	–	72	–	–	8923	3	3	17	63	1	–	–	18	1
	RH Int. 2 C1R6	2	58	–	–	8937	7	5	17	50	2	–	–	20	1
	RH Int. 1 C2R6	–	112	–	–	8833	13	12	21	75	2	–	–	21	2
	RH wing C3R6	21	–	–	–	6925	309	608	247	728	17	–	–	212	28
	RH wing C2R3	35	33	–	–	6963	305	582	198	729	9	–	<1	215	27

cm^{-3}. A detailed ToF HIERDA spectrum with both minor and major species detected on the surface of Tile 4D15, sample LH wing C1R4 is shown in Fig. 3. The main species, next to Be, are hydrogen isotopes, C, N, O and Inconel or steel components. In general, their contents are small, not exceeding the level of $1{\cdot}10^{18}$ cm^{-2}. The presence of W is detected, but the concentration is on the low level of 10^{16} cm^{-2}. The spatial distribution of co-deposits is not uniform over the tiles. The contents of noble (He, Ne, Ar) and other seeded gases on OPL are small in the central segments (Centre and Int. 2) most affected by plasma, while higher retention is on the wing and Int. 1 segment which can be considered as the deposition zones. In addition, it is stressed that the deposition of ^{3}He puffed in the main chamber is greater than other noble gases injected in the divertor. After ILW-3 ^{15}N is present all over the OPL tiles, while ^{18}O is found in only small amounts mainly in the wing area. Samples of similar toroidal positions (e.g. LH wing C1R4 on Tile 14 exposed to ILW-3 and Tile 15 exposed to ILW1–3) have a similar amount of species retained. The respective plasma times on the limiters were 106 min on Tile 14 during ILW-3 and 170 min on Tile 15 during ILW1–3 (of which 40 min during ILW-3) [3].

Fig. 4 shows depth profiles of species contained in the LH wing C1R4 of Tile 4D14 exposed to ILW-1 and, in the same position exposed to ILW-3. Species with very small concentrations (<0.5 atomic%), as well as Inconel or steel components are left out for clarity. The main constituents of the surfaces are Be, C, N O, and hydrogen isotopes. A careful comparison reveals several clear features and also differences. The retention of N doubled after the ILW-3 campaign, with $268{\cdot}10^{15}$ N cm^{-2}, compared to the retention after ILW-1 campaign, with $132{\cdot}10^{15}$ N cm^{-2}. This is associated with the overall seeding rate which approximately tripled from ILW-1 to ILW-3 (see Table 2). For such comparison it is important to consider the time of limiter plasma: for Tile 14 it was 141 min in ILW-1 and 106 min in ILW-3 [3]. ^{14}N is not detected (it is below the detection limit) at the very surface of the ILW-1 limiter, because the campaign was finished with 151 H-mode pulses when the limiter time was minimized to 25% of the total pulse duration [26]. The presence of ^{15}N is found only in the very surface layer after ILW-3. Its profile is steep

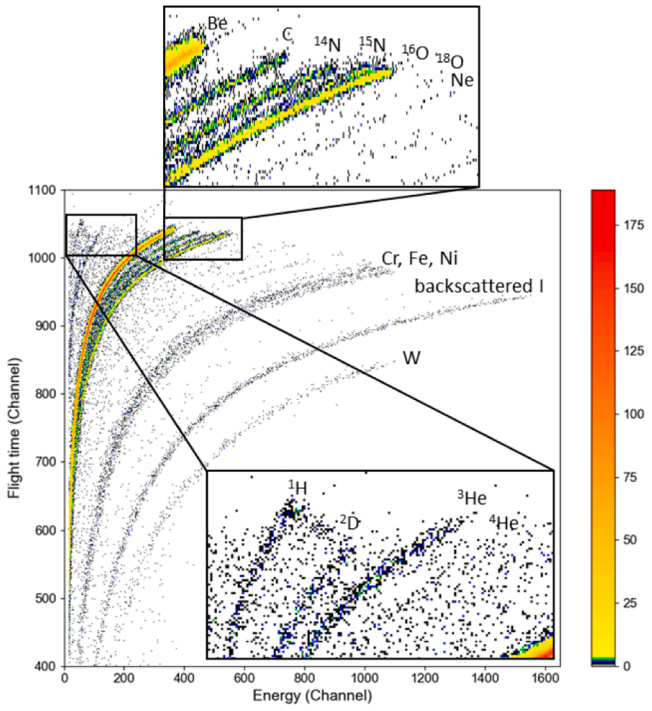

Fig. 3. ToF-HIERDA spectrum recorder with an iodine beam on the surface of OPL sample LH wing C1R4 from Tile 15 exposed to ILW1–3. Minor and major species are marked.

being consistent with the fact of seeding that gas in the final stage of the campaign.

In summary, the evidence that the nitrogen amount on the unexposed reference Be sample is below the detection limit, see Table 3, and the isotope ^{15}N was found on the surface after ILW-3, indicates that N on the limiters is indeed deposited in JET and, does not originate from the exposure to atmosphere. Small quantities of ^{3}He, below 1 atomic%, are also visible in Fig. 4. To authors knowledge it is the first report on the analysis of that isotope on PFC. Two other noble gases (Ne and Ar) are present in minute quantities, while Kr (puffed massively by DMV) and Xe are not detected.

The contents of C in the surface layer are similar (2–3 atomic%) in both samples. In the case of the ILW-3 sample, the presence of carbon may also be related to the injection of CD_4 from GIM 11 for transport studies during the last operation session. However, the most important are fairly small amounts of C. It may suggest that over the years, W coatings on the CFC tiles were not damaged, thus not creating an open carbon source. This is in line with other studies showing the decrease of carbon deposition in the divertor in consecutive campaigns [4,9]. The profiles for C, O (also ^{14}N in ILW-3) are approximately flat over the probed thickness thus indicating that the co-deposited layers are thicker than the region probed by HIERDA. The error in the assessment of C, N isotopes and O is on the level of 10–15%. However, for the species occurring in small amounts (1 atomic% or below) the error may be around 50% because of the poor statistics. The roughness determined on the samples Centre C4R4 and LH Int. 1 C2R4 from tile 4D14 exposed to ILW-3 are 0.8 μm and 1.4 μm, respectively. Increasing roughness reduces the depth resolution for HIERDA.

3.1.2. *Inner wall guard limiters*

Data obtained for the IWGL specimens from Tiles 10 and 11 located in Octant 2 are listed in Table 5. It is to be added that plasma touched Tile 11 during ILW1–3 for 316.5 min, which makes Tile 11 the most exposed region of the IWGL beam. Tile 10 was in contact with plasma for 104 min during ILW-1 and for 82.5 min during ILW-2. These data originate from measurements within 2 mm of limiter surfaces [3]. The contents of respective species (hydrogen isotopes, C, N, O, Inconel or steel components and W) on IWGL are in general in the similar range as found on the outer limiters. Similarly to OPL, also on the IWGL higher amounts of co-deposits are at the wing areas than in central parts of the tile. The exception to this behaviour is on the outermost column of the RH wing of both tiles (RH wing C1R4), where the N retention decreases. Comparing positions RH wing C4R7 and RH wing C3R4 of Tile 10 exposed to ILW-1 and ILW-2, the toroidal positions differing only by around 1 cm, the data suggest a similar amount of retained O and C. The N amount has more than tripled, with $84{\cdot}10^{15}$ cm^{-2} after ILW-1 and $261{\cdot}10^{15}$ cm^{-2} after ILW-2. The N seeding rate, see Table 2, has increased nearly by factor of 4.

The major difference between respective IWGL samples from consecutive campaigns is the amount of H, which is greater after ILW-2 than after the two other campaigns; the results are shown in Fig. 5. It reflects the fact of finishing the second campaign with 300 hydrogen-fuelled shots [4]. That diminished the amount of stored deuterium. However, during further operation (ILW-3) H was either exchanged by D or the deuterium-depleted layer was covered by a new D-containing co-deposit, as discussed in [5,27]. In addition, a pronounced profile of ^{15}N has been measured on the RH wing sample C3R7 exposed to ILW1–3.

3.1.3. *Dump plates*

Samples of DP from Octants 2 and 3 were examined; some of them with a clear melt damage. Results of ToF HIERDA measurements are collected in Table 6; molten samples are marked with an asterisk. They are characterized by much lower contents of O, C, ^{14}N, metals (Cr, Fe, Ni, Mo, W) and hydrogen isotopes than those not damaged. However, ^{15}N is found (below $10{\cdot}10^{15}$ cm^{-2}) only in the molten areas. This is probably

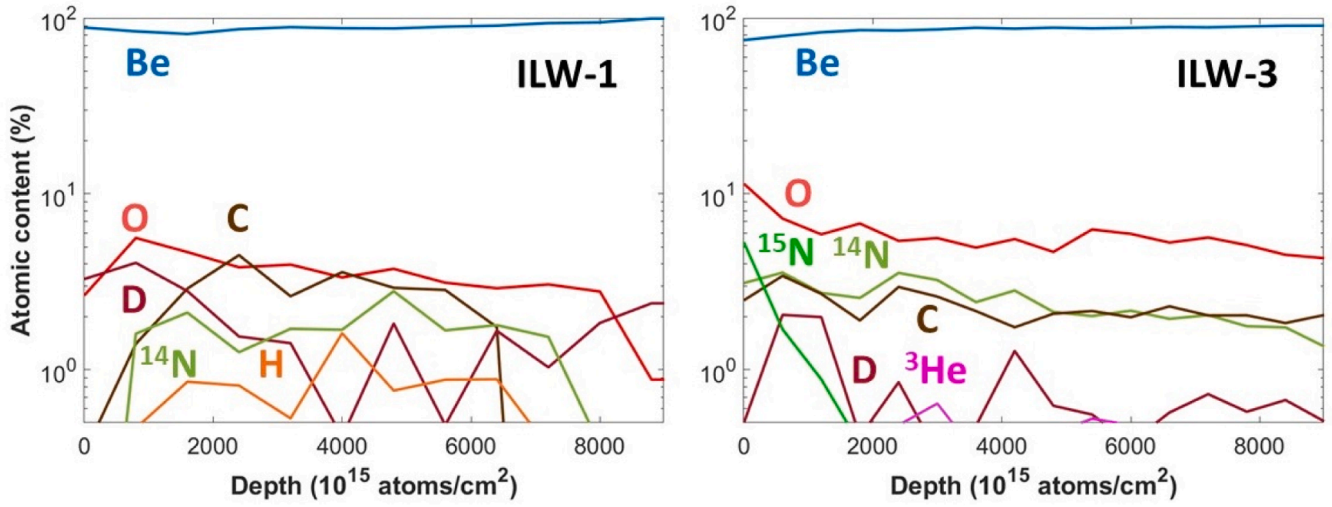

Fig. 4. Depth profiles of atomic content to a depth of $9{\cdot}10^{18}$ atoms cm^{-2} plotted logarithmically. Profiles of OPL position LH wing C1R4 exposed to ILW-1 (left) and ILW-3 (right).

Table 5
ToF HIERDA measurement results on PFS of samples from IWGL Tile 10 (2XR10) and 11 (2XR11) from Octant 2 exposed to ILW-1/ILW-2 and ILW1–3, respectively. Values given in 10^{15} atoms cm^{-2}. Measurement depth $9{\cdot}10^{18}$ atoms cm^{-2}, this corresponds to approximately 750 nm at assumed density of 1.803 g cm^{-3}.

Tile	Position	Areal density in 10^{15} atoms cm^{-2}										
		^{1}H	^{2}D	Be	C	^{14}N	^{15}N	^{16}O	^{18}O	Ar	Cr, Fe, Ni, Mo	W
2XR10 (ILW-1)	**RH wing C4R7**	61	90	7476	298	84	–	910	–	–	172	–
	Centre C7R2	14	–	8960	11	6	–	87	–	–	17	5
2XR10 (ILW-2)	**RH wing C1R4**	69	–	7677	166	103	–	948	–	–	122	15
	RH wing C3R4	185	–	7104	249	261	–	933	–	–	157	–
	Centre C6R4	15	29	8941	38	–	–	68	–	–	8	–
	Centre C6R5	29	–	8933	25	–	–	70	–	–	5	–
2XR11 (ILW1–3)	**RH wing C1R4**	19	45	8492	59	35	8	351	2	3	65	12
	RH wing C3R3	–	125	7461	268	470	232	450	8	3	70	5
	RH wing C3R7	8	135	7483	365	353	289	378	14	3	63	5
	Centre C5R4	–	10	9009	3	1	5	59	–	2	6	1
	LH Int. C1R4	–	–	8952	22	16	–	97	–	–	11	1
	LH Int. C3R4	16	113	7945	179	320	144	274	6	1	88	9

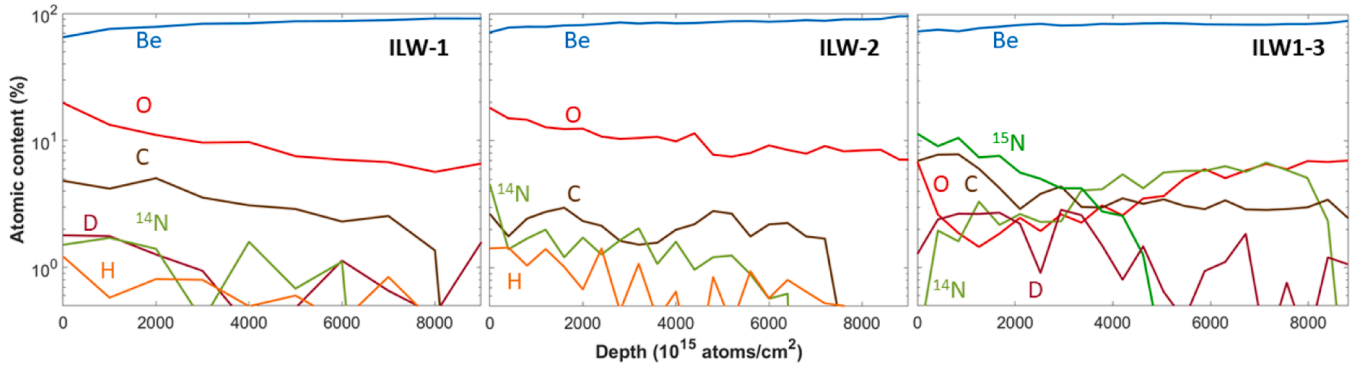

Fig. 5. Depth profiles of atomic content to a depth of $9{\cdot}10^{18}$ atoms cm^{-2} plotted logarithmically. Profiles of IWGL position RH wing C4R7 exposed to ILW-1, RH wing C1R4 exposed to ILW-2, and RH wing C3R7 exposed to ILW1–3.

attributed to the surface properties, i.e. highly developed surface, thus enabling efficient deposition of the isotope puffed in the last phase of the campaign.

The DP samples from column 2 and 5 on Tile 3A8 (ILW1–3) retain large amounts of O, Inconel or steel components and W, if compared with deposition areas on the OPL or IWGL. It can be connected with experiments on generation of runaway electrons at the end ILW-2, which caused serious modification of the DP structure and composition [19]. On some areas of Tile 3A8 ^{3}He is retained, locally up to $26{\cdot}10^{15}$ cm^{-2}. Ar is also detected, but the amounts are not higher than those measured on the machined reference Be sample, see Table 3.

The roughness of sample C2R9 and C5R12 from tile 3A8 was measured. The average measured roughness was 2.4 μm, similar for both samples. Three samples from Tile 3A8 (C2R9, C4R12, C5R12) were

Table 6
ToF HIERDA measurement results on samples of DP 8 (3A8) and 4 (2B4C) exposed to campaigns ILW1–3 and ILW-3, respectively. Values given in 10^{15} atoms cm^{-2}. Measurement depth to $9{\cdot}10^{18}$ atoms cm^{-2}, this corresponds to approximately 750 nm at the Be density of 1.803 g cm^{-3}.

Tile	Position	Areal density in 10^{15} atoms cm^{-2}											
		^{1}H	^{2}D	^{3}He	Be	C	^{14}N	^{15}N	^{16}O	^{18}O	Ar	Cr, Fe, Ni, Mo	W
2B4C (ILW-3)	**C6R2***	–	–	–	9053	1	1	2	30	1	4	6	1
	C6R8*	10	4	–	8855	14	6	9	144	–	5	28	5
3A8 (ILW1–3)	**C2R9**	30	66	–	7295	175	191	–	970	–	5	293	57
	C2R12	34	65	–	7021	171	236	–	1057	–	10	384	55
	C2R14	32	54	–	7098	176	256	–	1049	–	–	350	51
	C4R9*	<1	4	–	9012	3	3	3	57	–	1	12	1
	C4R12*	5	28	–	8698	21	61	7	224	–	10	37	5
	C5R9	18	115	19	6574	207	175	–	1515	–	12	369	60
	C5R12	21	127	26	6586	183	156	–	1550	–	14	356	56
	C5R14	23	117	26	6647	167	153	–	1487	–	11	380	59

* Molten samples.

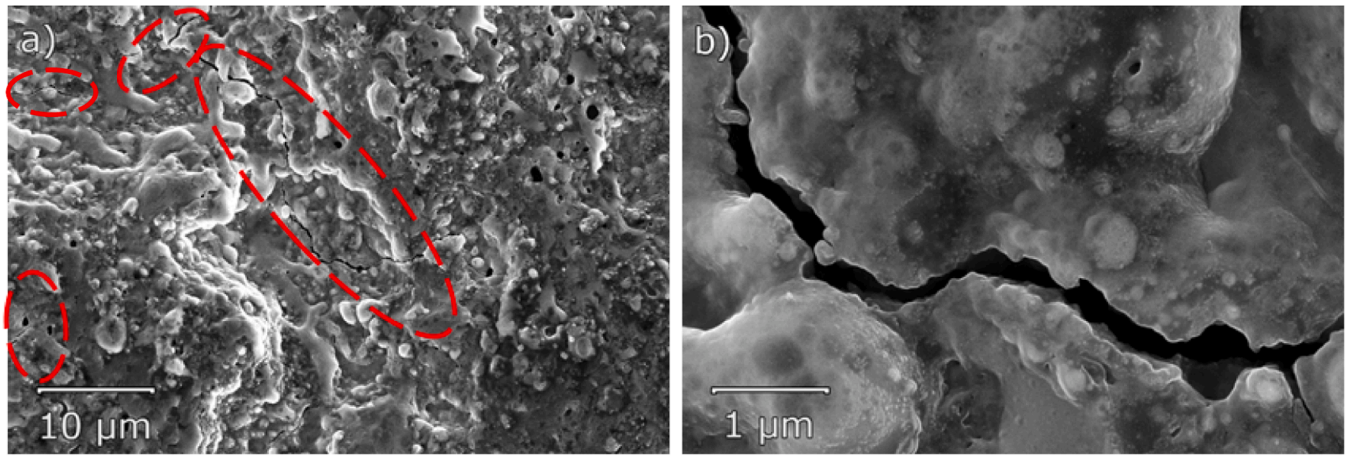

Fig. 6. Scanning electron microscopy image of cracked surface on sample C2R9, Tile 3A8. (a) Crack structures at 5 k X magnification (b) Crack at 50 k X magnification.

investigated with SEM. The results from sample C2R9 are in Fig. 6(a) and (b) in two magnifications, showing the network and dimensions of cracks. C5R12 did not show any cracks, despite the similar roughness as sample C2R9. Cracks were not an isolated occurrence, as they were also found on the molten sample C4R12.

3.2. Bulk tungsten divertor tile

The structure of Tile 5 is shown in Fig. 2(c). The examined samples originated from Stack A and Stack C. The outer strike point location on Tile 5 was mainly on Stacks C and D, while on Stack A it was located only for 201 s in ILW-1, 68 s in ILW-2 and 101 s in ILW-3. These are very short time spans compared to the divertor plasma times of several hours given in Table 1. The lamellae of Stack A are therefore considered to be cold.

ToF HIERDA data for the PFS of Tile 5 are collected in Table 7. Be is the major co-deposited species (up to $4{\cdot}10^{17}$ cm^{-2}) followed by C, O (in sum up to $4{\cdot}10^{17}$ cm^{-2}) and some ^{14}N. The presence of that isotope was found on all examined surfaces from the divertor, also on those from poloidal and toroidal gaps separating adjacent lamellae and stacks. Neither nitrogen-15, puffed from GIM 10, nor oxygen-18, from GIM 11, are detected on the bulk W. Even though both species have been found on W/CFC divertor tiles exposed to ILW-3 and on the wall probes, especially ^{18}O in the latter case (up to $2{\cdot}10^{16}$ cm^{-2}) [25,28]. However, in the case of W/CFC, ^{18}O feature is locally detected, but the actual

Table 7
ToF HIERDA measurement results on PFS of Tile 5 divertor samples exposed to ILW campaign 2, 1–3 and 3, respectively. Values given in 10^{15} atoms cm^{-2}. Measurement depth $2{\cdot}10^{18}$ atoms cm^{-2}, this corresponds to approximately 315 nm at the tungsten density of 19.29 g cm^{-3}.

Campaign	Lamellae	Areal density in 10^{15} atoms cm^{-2}									
		^{1}H	^{2}D	^{3}He	^{4}He	Be	C	^{14}N	^{16}O	Cr, Fe, Ni	W
ILW-2	**C3**	42	25	–	–	308	173	80	162	–	1300
	C23	23	–	44	12	217	211	41	107	–	1445
ILW1–3	**A23**	13	16	–	–	111	163	26	174	31	1526
	A24	6	10	2	–	74	100	8	85	–	1815
	C2	13	39	–	–	179	172	44	212	39	1349
	C12	–	42	–	–	418	188	168	196	49	1038
	C13*	9	30	–	–	247	122	71	165	15	1431
	C23	27	121	19	–	286	126	77	135	–	1296
	C24	3	2	5	–	78	41	14	42	–	1915

* Exposure to ILW-3 only.

amounts cannot be quoted with a reasonable level of confidence because of the high surface roughness.

The retention of H and D on the examined lamellae does not exceed (with one exception on C23) the level of $40{\cdot}10^{15}$ cm^{-2}. H contents after ILW-2 are greater than the D amount after that campaign. The sample C23 exposed to ILW-2 contains no D at all in the first 300 nm; the reason was discussed in Section 3.1.2. In general, more deposits are found on Stack C where the outer strike point was frequently located than on Stack A weakly affected by plasma loads. The deposition on Stack C is fairly uniform with an exception of lamella C24 (ILW1–3), i.e. the place with the greatest heat load on Tile 5. It is stressed that the retention of helium (especially ^{3}He) is found only on those two hot rows of lamellae (23 and 24) in the tile. It may tentatively be suggested that some helium incoming with the background plasma flux migrated into the metal and remained there. This statement is partly supported by the depth profile of ^{3}He in C23 from ILW-2, as shown in Fig. 7. Also the contents of H, ^{4}He and ^{14}N decrease with the increasing depth. The profiles of Be, C, O are fairly flat just indicating thicker deposits than the probed surface layer of 300 nm. The same trend has been observed in several profiles for samples from both campaigns.

A family of other than He noble gases (Ne, Ar, Kr, Xe) is not represented at all on the PFS of Tile 5; only minute amount of Ar, $<10^{16}$ cm^{-2}, was detected on the poloidal and toroidal gap surfaces, but not on PFS. The gases are absent despite being puffed from the divertor GIM for plasma-edge cooling and massive injection for disruption mitigation, e.g. 10^{25} level for Ar and Kr in ILW-3. It indicates that only species present in a regular plasma discharge modify surfaces and are retained there by co-deposition involving implantation.

4. Discussion

The motivation steamed from the interest, whether the amount of gases accumulated in the wall could be a threat to the operation, like in the case of nitrogen accumulation in a carbon wall machine [1,16]. When respective ILW campaigns are compared, the retention level of ^{14}N is found approximately proportional to the seeding rate, especially in the case of frequent puffing, as in ILW-3. On beryllium limiters, nitrogen is one major surface constituent: up to 10 atomic%, $6{\cdot}10^{17}$ cm^{-2}. The experiment with ^{15}N marker injections at the last sessions of ILW-3 clearly shows that the species accounts for more than 10 atomic% of surface composition in Be, at least temporarily. The species is transported even to the top region of the main chamber where it could be detected on the dump plates. However, ^{15}N is not found on the bulk W divertor tile, i.e. in the region where the gas was seeded. Also, the amounts of ^{14}N on that tile are significantly lower than on the Be limiters. The latter results are consistent with data obtained for metal wall probes (covers of quartz microbalance and test mirrors) from the JET divertor: only small quantities of ^{14}N [25] and no ^{15}N marker have been found [25,28]. Therefore, it is tentatively suggested that the nitrogen accumulation on and/or in high-Z wall components is lower than in the surface layer of Be. The content of nitrogen significantly exceeds, by a factor of 2 up to 10, the amount of retained fuel species. The exact N retention rate, for the reason discussed later, cannot be given with a high level of confidence, but the obtained results indicate a level of not less than a few % of the total N_2 feed, while the overall D retention reaches only 0.2% [5].

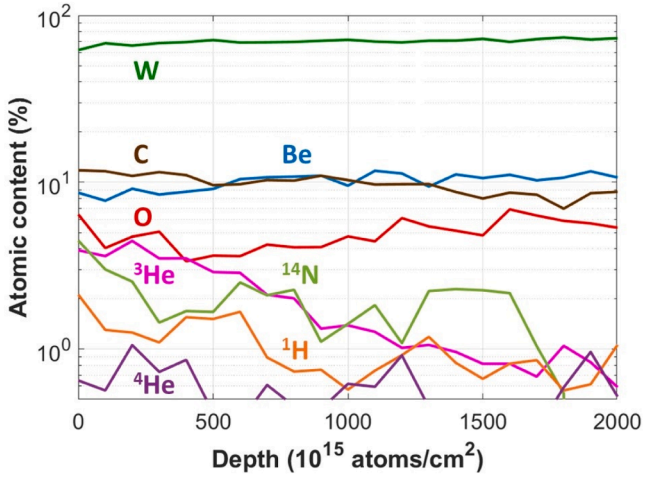

Fig. 7. Depth profiles of atomic content to a depth of $2{\cdot}10^{18}$ atoms cm^{-2} plotted logarithmically. Profiles for a sample from lamella C23 exposed to ILW-2.

The experiment with ^{18}O has proven the transport from the divertor and effective sticking of oxygen to wall components in the main chamber (Be limiters), and also to the wall probes in the divertor [25,28]. The fact itself is not surprising, but it should be kept in mind that only $2.8{\cdot}10^{22}$ atoms were injected in five shots and up $2{\cdot}10^{16}$ cm^{-2} were deposited in some regions.

The presence of helium isotopes on PFC surfaces from all studied regions of JET is shown for the first time. The amounts of ^{3}He are clearly above the detection limit and a depth profile could be determined on the bulk tungsten tile (Table 7, Fig. 7) with Be, C and N deposit. Taking the chemical inertness of helium into account, it can be only tentatively considered that its presence stems from a shallow co-implantation followed by the in-depth migration into a material. It is only a hypothesis, but it is based on the fact that other noble gases of bigger atomic dimensions are either not detected or in tiny numbers, like Ne which was puffed in larger quantities than He. It is also stressed that Ne, Ar and Kr despite massive injection by DMV, e.g. $1.3{\cdot}10^{25}$ Kr atoms in ILW-3, are absent on the examined surfaces thus proving that they did not enter the co-deposition or implantation mechanism. In a consequence, DMV have minor impact on the PFC composition. Both mitigation methods deliver gas which is neutral to the layers.

In summary, the deposition of minor species (noble gases, nitrogen and tracer gases) has been clearly proven. Local presence and depth distribution have been assessed. However, the gas balance for respective gases cannot be attempted. The statistics is low and this bears a risk of a significant data scatter and, eventually, could lead to too superficial or speculative conclusions what should be avoided.

5. Concluding remarks

The contribution of this work to the field of material migration and PFC composition is at least twofold. For the first time ever, such comprehensive analyses of the seeded noble and tracer gases in a metal wall tokamak have been performed. The deposition and retention in various classes of limiter and divertor materials has been assessed. This has been possible due to the availability of specimens from the four distinct locations in JET torus after three consecutive ILW campaigns, and the use of ToF-HIERDA for tracing constituents, from H to W, in the first few hundreds of nanometers of the samples. Secondly, significant nitrogen accumulation on PFC has been shown. The retention of ^{15}N and the comparison to the unexposed reference sample proves that the detected nitrogen is deposited in JET and not from atmosphere during the retrieval and long-term storage of PFC in air. The retention of both He isotopes on metal PFC has been determined. It is difficult to associate that with the presence of any W fuzz on the surface, but it may be rather related to the in-depth migration of He into the bulk material. Last but not least, the data show very limited (if any) impact of other noble gases injected for disruption mitigation on the surface state of wall components.

Data availability statement

The data presented in this study are available on reasonable request from the corresponding author.

Declaration of Competing Interest

The authors declare that they have no known competing financial interests or personal relationships that could have appeared to influence the work reported in this paper.

Data availability

Data will be made available on request.

Acknowledgements

This work has been carried out within the framework of the EUROfusion Consortium, funded by the European Union via the Euratom Research and Training Programme (Grant Agreement No 101052200 — EUROfusion). Views and opinions expressed are however those of the author(s) only and do not necessarily reflect those of the European Union or the European Commission. Neither the European Union nor the European Commission can be held responsible for them. The work has been supported by the Swedish Research Council (VR) [Grant 2015–04844 and 2016–05380]. Financial support of the Tandem Accelerator Infrastructure by VR-RFI [Grant 2017–00646_9, 2019_00191] as well as the Swedish Foundation for Strategic Research (SSF) under contract RIF14–0053 is gratefully acknowledged.

References

[1] A. Weckmann, P. Petersson, M. Rubel, P. Wienhold, S. Brezinsek, J.W. Coenen, A. Kirschner, A. Kreter, A. Pospieszczyk, Local migration studies of high- *Z* metals in the TEXTOR tokamak, Physica Scripta T167 (2016), 014058, https://doi.org/10.1088/0031-8949/T167/1/014058.

[2] G.F. Matthews, M. Beurskens, S. Brezinsek, M. Groth, E. Joffrin, A. Loving, M. Kear, M.-L. Mayoral, R. Neu, P. Prior, V. Riccardo, F. Rimini, M. Rubel, G. Sips, E. Villedieu, P. de Vries, M.L. Watkins, EFDA-JET contributors, JET ITER-like wall—overview and experimental programme, Physica Scripta T145 (2011), 014001, https://doi.org/10.1088/0031-8949/2011/T145/014001.

[3] A. Widdowson, S. Aleiferis, E. Alves, L. Avotina, A. Baron-Wiechec, N. Catarino, J. P. Coad, V. Corregidor, K. Heinola, I. Jepu, C. Makepeace, J.E.T. Contributors, Fuel inventory and material migration of JET main chamber plasma facing components compared over three operational periods, Physica Scripta T171 (2020), 014051, https://doi.org/10.1088/1402-4896/ab5350.

[4] S. Krat, M. Mayer, A. Baron-Wiechec, S. Brezinsek, P. Coad, Y. Gasparyan, K. Heinola, I. Jepu, J. Likonen, P. Petersson, C. Ruset, G. de Saint-Aubin, A. Widdowson, JET contributors, comparison of erosion and deposition in JET divertor during the first three ITER-like wall campaigns, Physica Scripta T171 (2020), 014059, https://doi.org/10.1088/1402-4896/ab5c11.

[5] A. Widdowson, J.P. Coad, Y. Zayachuk, I. Jepu, E. Alves, N. Catarino, V. Corregidor, M. Mayer, S. Krat, J. Likonen, K. Mizohata, C. Rowley, M. Zlobinski, M. Rubel, D. Douai, K. Heinola, T. Wauters, L. Dittrich, S. Moon, P. Petersson, A. Baron-Wiechec, L. Avotina, Evaluation of tritium retention in plasma facing components during JET tritium operations, Physica Scripta 96 (2021), 124075, https://doi.org/10.1088/1402-4896/ac3b30.

[6] T. Loarer, S. Brezinsek, V. Philipps, J. Bucalossi, D. Douai, H.G. Esser, S. Grunhagen, J. Hobirk, S. Jachmich, E. Joffrin, U. Kruezi, C. Lowry, G. Matthews, R. Smith, E. Tsitrone, S. Vartanian, Comparison of long term fuel retention in JET between carbon and the ITER-Like Wall, J. Nucl. Mater. 438 (2013) S108–S113, https://doi.org/10.1016/j.jnucmat.2013.01.017.

[7] S. Krat, M. Mayer, J.P. Coad, C.P. Lungu, K. Heinola, A. Baron-Wiechec, I. Jepu, A. Widdowson, Comparison of JET inner wall erosion in the first three ITER-like wall campaigns, Nucl. Mater. Energy 29 (2021), 101072, https://doi.org/10.1016/j.nme.2021.101072.

[8] S. Glöggler, Experimental and Numerical Investigation of Neon-Seeded High Radiation Discharges At the JET Tokamak, Technische Universität München, 2022. https://mediatum.ub.tum.de/doc/1639792/1639792.pdf.

[9] J. Mailloux, et al., Overview of JET results for optimising ITER operation, Nucl. Fusion. (2022) 62, https://doi.org/10.1088/1741-4326/ac47b4.

[10] P. Petersson, M. Rubel, H.G. Esser, J. Likonen, S. Koivuranta, A. Widdowson, Co-deposited layers in the divertor region of JET-ILW, J. Nucl. Mater. 463 (2015) 814–817, https://doi.org/10.1016/j.jnucmat.2014.12.077.

[11] M. Rubel, A. Weckmann, P. Ström, P. Petersson, A. Garcia-Carrasco, S. Brezinsek, J. Coenen, A. Kreter, S. Möller, P. Wienhold, T. Wauters, E. Fortuna-Zaleśna, Tracer techniques for the assessment of material migration and surface modification of plasma-facing components, J. Nucl. Mater. 463 (2015) 280–284, https://doi.org/10.1016/j.jnucmat.2014.11.074.

[12] E. Fortuna-Zaleśna, J. Grzonka, M. Rubel, A. Garcia-Carrasco, A. Widdowson, A. Baron-Wiechec, L. Ciupiński, J.E.T. Contributors, Studies of dust from JET with the ITER-Like Wall: composition and internal structure, Nucl. Mater. Energy 12 (2017) 582–587, https://doi.org/10.1016/j.nme.2016.11.027.

[13] J.F. Ziegler. Handbook of Ion Implantation Technology, North-Holland, Amsterdam, New York, 1992. https://www.worldcat.org/title/handbook-of-ion-implantation-technology/oclc/26308931.

[14] G. Federici, C.H. Skinner, J.N. Brooks, J.P. Coad, C. Grisolia, A.A. Haasz, A. Hassanein, V. Philipps, C.S. Pitcher, J. Roth, W.R. Wampler, D.G. Whyte, Plasma–material interactions in current tokamaks and their implications for next step fusion reactors, Nucl. Fusion 41 (2001), 1967, https://doi.org/10.1088/0029-5515/41/12/218.

[15] M. Oberkofler, G. Meisl, A. Hakola, A. Drenik, D. Alegre, S. Brezinsek, R. Craven, T. Dittmar, T. Keenan, S.G. Romanelli, R. Smith, D. Douai, A. Herrmann, K. Krieger, U. Kruezi, G. Liang, C. Linsmeier, M. Mozetic, V. Rohde, the ASDEX Upgrade team, the EUROfusion MST1 Team, JET Contributors, Nitrogen retention mechanisms in tokamaks with beryllium and tungsten plasma-facing surfaces, Physica Scripta T167 (2016), 014077, https://doi.org/10.1088/0031-8949/T167/1/014077.

[16] M. Rubel, V. Philipps, L. Marot, P. Petersson, A. Pospieszczyk, B. Schweer, Nitrogen and neon retention in plasma-facing materials, J. Nucl. Mater. 415 (2011) S223–S226, https://doi.org/10.1016/j.jnucmat.2010.08.035.

[17] U. Kruezi, S. Jachmich, H.R. Koslowski, M. Lehnen, S. Brezinsek, G. Matthews, A new disruption mitigation system for deuterium–tritium operation at JET, Fusion Eng. Des. 96–97 (2015) 286–289, https://doi.org/10.1016/j.fusengdes.2015.06.109.

[18] S. Jachmich, P. Drewelow, S. Gerasimov, U. Kruezi, M. Lehnen, C. Reux, V. Riccardo, I. Carvalho, A. Pau, M. Imsirek, E. Joffrin, Disruption mitigation at JET using massive gas injection. 43rd EPS Conf. on Plasma Physics, 2016. http://ocs.ciemat.es/EPS2016PAP/pdf/O4.123.pdf.

[19] I. Jepu, G.F. Matthews, A. Widdowson, M. Rubel, E. Fortuna-Zaleśna, J. Zdunek, P. Petersson, V. Thompson, P. Dinca, C. Porosnicu, P. Coad, K. Heinola, N. Catarino, O.G. Pompilian, C.P.L. and, Beryllium melting and erosion on the upper dump plates in JET during three ITER-like wall campaigns, Nucl. Fusion. 59 (2019), 086009, https://doi.org/10.1088/1741-4326/ab2076.

[20] A. Huber, S. Brezinsek, V. Huber, E.R. Solano, G. Sergienko, I. Borodkina, S. Aleiferis, A. Meigs, D. Tskhakaya, M. Sertoli, M. Baruzzo, D. Borodin, P. Carvalho, E. Delabie, D. Douai, A. Kirschner, K. Lawson, C. Linsmeier, J. Mailloux, S. Menmuir, P. Mertens, E. Pawelec, J. Romazanov, A. Shaw, Understanding tungsten erosion during inter/intra-ELM periods in He-dominated JET-ILW plasmas, Physica Scripta 96 (2021), 124046, https://doi.org/10.1088/1402-4896/ac2d85.

[21] P. Ström, D. Primetzhofer, Ion beam tools for nondestructive in-situ and in-operando composition analysis and modification of materials at the Tandem Laboratory in Uppsala, J. Inst. 17 (2022) P04011, https://doi.org/10.1088/1748-0221/17/04/P04011.

[22] H.J. Whitlow, G. Possnert, C.S. Petersson, Quantitative mass and energy dispersive elastic recoil spectrometry: resolution and efficiency considerations, Nucl. Instrum. Methods Phys. Res. Sect. B 27 (1987) 448–457, https://doi.org/10.1016/0168-583X(87)90527-1.

[23] P. Ström, P. Petersson, M. Rubel, G. Possnert, A combined segmented anode gas ionization chamber and time-of-flight detector for heavy ion elastic recoil detection analysis, Rev. Scientific Instrum. 87 (2016), 103303, https://doi.org/10.1063/1.4963709.

[24] K. Arstila, J. Julin, M.I. Laitinen, J. Aalto, T. Konu, S. Kärkkäinen, S. Rahkonen, M. Raunio, J. Itkonen, J.-P. Santanen, T. Tuovinen, T. Sajavaara, Potku – new analysis software for heavy ion elastic recoil detection analysis, Nucl. Instrum. Methods Phys. Res. Sect. B 331 (2014) 34–41, https://doi.org/10.1016/j.nimb.2014.02.016.

[25] P. Ström, P. Petersson, M. Rubel, E. Fortuna-Zaleśna, A. Widdowson, G. Sergienko, Analysis of deposited layers with deuterium and impurity elements on samples from the divertor of JET with ITER-like wall, J. Nucl. Mater. 516 (2019) 202–213, https://doi.org/10.1016/j.jnucmat.2018.11.027.

[26] S. Brezinsek, T. Loarer, V. Philipps, H.G. Esser, S. Grünhagen, R. Smith, R. Felton, J. Banks, P. Belo, A. Boboc, J. Bucalossi, M. Clever, J.W. Coenen, I. Coffey, S. Devaux, D. Douai, M. Freisinger, D. Frigione, M. Groth, A. Huber, J. Hobirk, S. Jachmich, S. Knipe, K. Krieger, U. Kruezi, S. Marsen, G.F. Matthews, A.G. Meigs, F. Nave, I. Nunes, R. Neu, J. Roth, M.F. Stamp, S. Vartanian, U.S. and, Fuel retention studies with the ITER-Like Wall in JET, Nucl. Fusion. 53 (2013), 083023, https://doi.org/10.1088/0029-5515/53/8/083023.

[27] L. Dittrich, P. Petersson, M. Rubel, T.T. Tran, A. Widdowson, I. Jepu, C. Porosnicu, E. Alves, N. Catarino, J.E.T. Contributors, Fuel retention and erosion-deposition on inner wall cladding tiles in JET-ILW, Physica Scripta 96 (2021), 124071, https://doi.org/10.1088/1402-4896/ac379e.

[28] S. Moon, P. Petersson, M. Rubel, E. Fortuna-Zalesna, A. Widdowson, S. Jachmich, A. Litnovsky, E. Alves, First mirror test in JET for ITER: complete overview after three ILW campaigns, Nucl. Mater. Energy 19 (2019) 59–66, https://doi.org/10.1016/j.nme.2019.02.009.